ADVANCED OPTICAL MATERIALS
www.advopticalmat.de

Photoexcitation Control of Excitation Relaxation in Mixed-Phase Ruddlesden-Popper Hybrid Organic-Inorganic Lead-Iodide Perovskites

*Anna Stadlbauer, Lissa Eyre, Alexander Biewald, Felix Rauh, Markus W. Heindl, Shangpu Liu, Jonathan Zerhoch, Sascha Feldmann, Achim Hartschuh, and Felix Deschler**

The electronic states and exciton binding energies of layered Ruddlesden-Popper (RP) metal-halide perovskites can be tailored through changes of their chemical composition, yielding multi-phase systems with complex energy cascades. Ultrafast photoexcitation relaxation with transfer dynamics into domains of increasing layer number has been reported for these materials. Here, ultrafast optical spectroscopy is used to report an unexpected excitation energy dependence of photoexcitation relaxation dynamics in mixed-dimensional benzylammonium cesium lead iodide RP perovskite ($BeA_2CsPb_2I_7$) thin films, which gives rise to spectrally broadband luminescence over the visible region. Using transient absorption and photoluminescence spectroscopy it is found that excitations, which are formed in the $n = 2$ RP-phase after photoexcitation with ≈0.2 electron volt excess energy, transfer to higher layer number RP-phases on unexpectedly slow timescales of tens of picoseconds. Further, it is observed that such excitations are initially optically passive. Notably, luminescence occurs under these conditions from multiple RP-phases with optical bandgaps across the visible range, yielding broadband luminescence. The results hold potential for realization of broadband white-light emitters and other light-emitting devices.

1. Introduction

Mixed-phase Ruddlesden-Popper (RP) hybrid metal-halide perovskites with structural formula $A_2B_{n-1}Pb_nI_{3n+1}$ (with n = *1,2,3,4,...,∞*) form excitons at room temperature and show strong photoluminescence (PL) with a narrow linewidth. By tuning the material composition, the number of repeating lead-halide octahedra in the inorganic layers *n*, often also called "layer number" or "phase" of the Ruddlesden-Popper series, can be tailored, providing a broad parameter space to control the optoelectronic properties of these materials.[1–4] For layer numbers larger than $n = 5$, the behavior of the photo-excitations was interpreted as free-carrier like, as, e.g., in bulk metal-halide perovskites, while for phases with lower "*n*"-number, excitonic properties gradually start to play a dominant role.[2]

The excitation with an energy larger than the bandgap of the investigated semiconductor may result in the formation of

A. Stadlbauer, M. W. Heindl, S. Liu, J. Zerhoch, F. Deschler
Institute of Physical Chemistry
University of Heidelberg
Im Neuenheimer Feld 229, 69120 Heidelberg, Germany
E-mail: deschler@uni-heidelberg.de

A. Stadlbauer, L. Eyre, F. Rauh, M. W. Heindl
Walter Schottky Institute
Technical University of Munich
Am Coulombwall 4, 85748 Garching, Germany

A. Stadlbauer, F. Rauh, M. W. Heindl
Physics Department, TUM School of Natural Sciences
Technical University of Munich
Am Coulombwall 4, 85748 Garching, Germany

L. Eyre
Electrical Engineering Division
University of Cambridge
9 JJ Thomson Ave, Cambridge CB3 0FA, UK

A. Biewald, A. Hartschuh
Department Chemistry and CeNS
Ludwig-Maximilians-Universität Munich
Butenandstr. 11, Haus E, 81377 München, Germany

S. Feldmann
Rowland Institute
Harvard University
100 Edwin H Land Boulevard, Cambridge, MA 02142, USA

The ORCID identification number(s) for the author(s) of this article can be found under https://doi.org/10.1002/adom.202301331

DOI: 10.1002/adom.202301331

free carriers and Coulomb-bound electron-hole pairs with excess energy above the band gap with an initial temperature above the lattice temperature. Via carrier-carrier-scattering during thermalization and afterward via carrier-phonon-scattering during the cooling, these so-called "hot excitons" or "hot carriers" reduce their energy.[5–8] For mixed-phase low-dimensional perovskites, excitons can experience ultrafast energy transfer to reach the band gap level.[6,8]

Exciton states which recombine non-radiatively, or which are optically passive, are often called dark states.[9,10] In the last years, these dark states in perovskites were intensively investigated since understanding and controlling such states and non-radiative recombination is key for high luminescence yields and potential applications in lighting.[9] Further, understanding the splitting between bright and dark states enables insight into the thermal population of a perovskite.[11] In semiconductors, the lowest excitonic state is dark, which results from the excitonic fine structure due to exchange interactions of spins from holes and electrons.[11,12] Being already at the lowest excitonic state, the dark state typically is a long-lived state due to a low direct recombination rate.[10,12] Increasing, e.g., photoluminescence signal from dark states, the so-called brightening of the dark states, as well as influencing their lifetimes can be performed using a strong magnetic field by influencing the dark and bright states as well by changing the temperature to cryogenic temperatures.[10,11,13]

Brightening of states can also be realized by populating the singlet state instead of the triplet state. In general, the lowest exciton level can be assumed to be a triplet state.[14] Since low *n*-phases exhibit a higher exciton-binding energy than higher *n*-phases, for them the singlet-triplet-splitting is more pronounced.[11] Consequently, the relative population of the triplet states is higher in low n-phases, since once hot carriers have cooled into the low-energy triplet state, a transition back into the higher energy singlet state (reverse intersystem crossing) is limited at room temperature. The triplet states created this way are considered dark, since their direct radiative recombination is spin-forbidden according to the Pauli principle.[14] The existence and the impact of singlet and triplet states in low-dimensional materials and in different perovskite materials has been investigated by several groups providing different approaches how to overcome the splitting and hence improve the emission.[14-18]

For low-dimensional semiconductors, enhancing the photoluminescence is not only possible via transitions between singlet-triplet states but also via phonon-assisted radiative recombination.[19–22]

Furthermore, efficient transfer processes are crucial for bright luminescence. Different charge and energy transfer processes have been described for perovskite materials. Charge transfer requires structures with donor and acceptor type – which can depend on the band structure of different perovskite phases – to enable the transfer of a single charge. Energy transfer can be realized for example via Forster resonance energy transfer (FRET), Dexter energy transfer or via energy funneling. For distinguishing the processes not only the decay times but also the optical properties can be helpful.[17,23–27]

While manifold approaches for perovskite light emitting diodes (LEDs) have been successfully investigated in the last years,[28–31] there are still many challenges for the fabrication of blue perovskite LEDs.[28,30,32] Since the lack of blue perovskite LEDs prevents the fabrication of white perovskite LEDs based on a combination of perovskite RGB LEDs, the white spectrum of potential white perovskite LEDs needs to stem from a broad spectrum emitted from a suitable material or combination of materials.[28,30] Controlling the photoluminescence from different phases in a perovskite could be an approach for perovskite lightening applications such as broadband or white LEDs.

2. Results and Discussion

In our study, we have chosen to investigate thin films of the RP hybrid perovskite $A_2B_1Pb_2I_7$ where A = benzylammnonium ($C_7H_{10}N^+$) is the large organic molecule cation and B = Cs is the small inorganic cation. Based on the stoichiometry of the precursor solution, a sample with $(BeA)_2CsPb_2I_7$ would be predicted to be $n = 2$ phase, however, by tuning the fabrication parameters (see Supporting Information), we will show that a mixed phase thin film sample can be obtained (**Figure 1**).

2.1. Optical Properties of $(BeA)_2CsPb_2I_7$

A schematic of the expected structure of the RP hybrid perovskite is shown in Figure 1a. The upper part of this sketch presents the expected $n = 2$ structure with a double layer of the lead-iodide octahedra, while the lower part shows the structure for phases with $n \geq 2$, in which there are now several layers of the lead-halide octahedra. We characterized the crystal structure of our material with X-ray diffraction (XRD) (Figure S1, Supporting Information) and find evidence of a mixed phase composition.

First, we study the optical response from our sample with absorption and photoluminescence experiments (Figure 1b), which show multiple peaks from different RP phases. Based on previously reported work,[2] we assign the absorption features to different RP phases of the sample. The $n = 1$ phase is located at 520 nm, the $n = 2$ phase is at 565 nm and the $n = 3$ phase is at ≈615 nm.[2] The signal from $n = 2$ and $n = 3$ can be observed in both, the absorption spectrum and the PL spectrum. The specific distribution of phases in the PL spectra can be controlled via multiple parameters as for instance the annealing temperature (Figure S2, Supporting Information).

PL experiments at a fluence of ≈10 μJ cm^{-2} and excitation wavelength of 400 nm (Figure 1b) show a broad spectrum that covers the visible range. Higher *n*-number phases usually combine into a broad, red-shifted PL signal from about 630 to 725 nm, and due to the small energetic shifts between their signals,[2] we cannot clearly distinguish the individual phases. This indicates that the PL signal is a combination of the different phases in our mixed-phase films. Notably, such a broad spectrum with similar PL intensities from different phases is surprising, since fast relaxation to the lowest energy phase (i.e., highest *n*-number RP) could be expected due to the reported ultrafast cascading in the manifold of the RP phases.[33,34] A series of experiments at increasing fluences shows that the relative amount of the emitted signal of each phase, relative to the overall PL signal strongly depends on the fluence used for the excitation (Figure 1d). The equations for the fluence and the related initial carrier density are described in

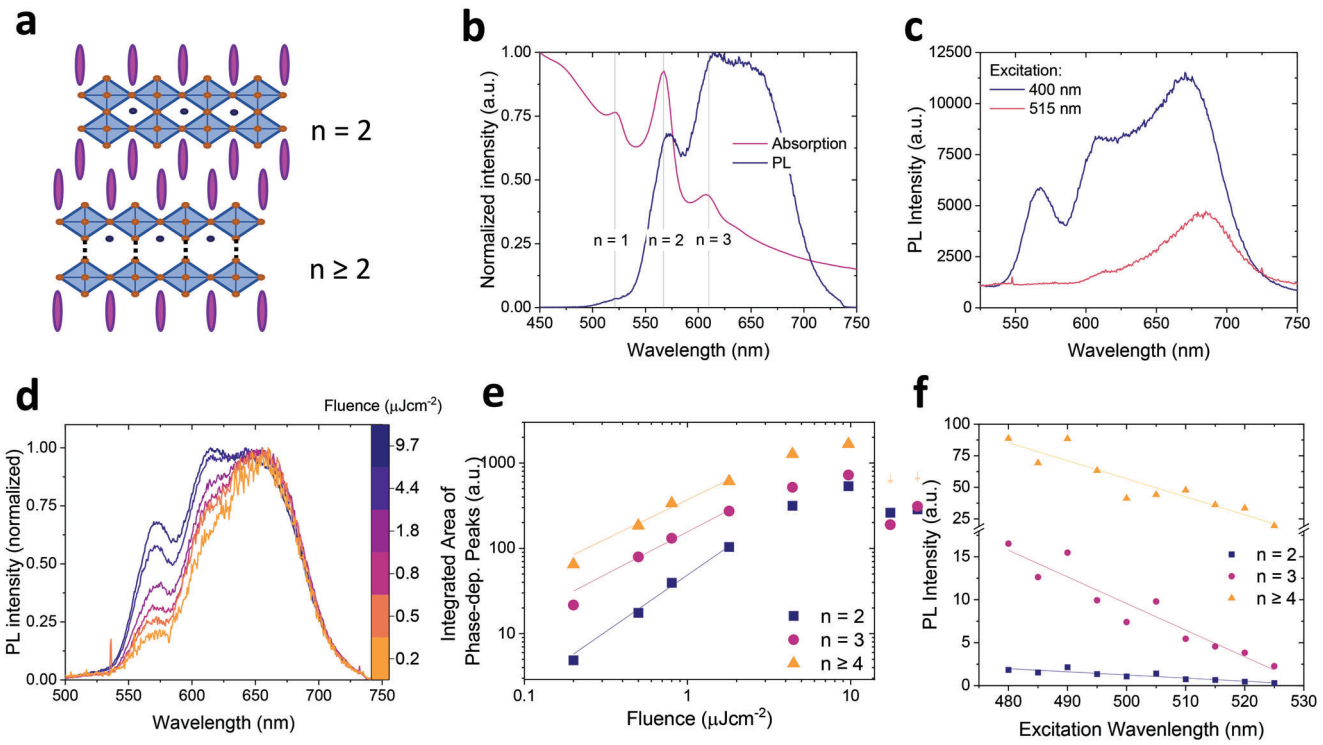

Figure 1. Optical properties of multi-phasic $(BeA)_2CsPb_2I_7$ RP hybrid perovskite thin films: a): Schematic of RP hybrid perovskite crystal structure. The *n*-number typically refers to the number of lead-iodide-octahedra layers between organic parts. The blue octahedra with orange dots represent the lead iodide layers, which are enclosing Cs atoms (dark blue). Between these inorganic layers sits a double layer of benzylammonium spacers (purple). b): Absorption and PL spectra (excitation at 400 nm) showing the presence of multiple RP phases. c): PL spectra for excitation at 400 and 515 nm showing excitation-dependent broadening for the higher energy wavelength. d): Fluence-dependent PL spectra (400 nm excitation) with spectral broadening on the high energy side for higher fluences, due to increasing signal from lower *n*-value RP phases. e): Fluence dependence of the contribution of different RP phases to the overall PL intensity. f): Impact of different excitation wavelengths on the relative PL intensities of the different n-phases.

the Supporting Information. Increasing the fluence broadens the spectrum from ≈85 nm full width half maximum (FWHM) for 0.2 μJ cm^{-2} to 128 nm for ≈10 μJ cm^{-2} (Figure S3, Supporting Information).

To extract the relative contribution of each phase of the RP series, we fit the PL spectra with a sum of three Gaussians for the phases $n = 2$, $n = 3$ and $n \geq 4$ (Figure S4, Supporting Information). This fit was performed for all PL spectra in the fluence series in order to analyze the fluence dependence of the contribution from the different phases. The fitted PL intensity for the different phases is shown in Figure 1e. Here (Figure 1e), we obtain a linear behavior for all phases for fluences smaller than 2 μJ cm^{-2} with a slope of ≈1.3 for the $n = 2$ phase. The slopes of ≈0.99 for the $n = 3$ phase and ≈0.92 for the $n \geq 4$ phase are close to the value 1 of the power index which indicates monomolecular recombination.[9] These values of the slopes prove, that we find more PL from the $n = 2$ phase for higher excitation density. This indicates that some process is outcompeting the cascading from the $n = 2$ phase. For higher fluences of up to ≈10 μJ cm^{-2}, saturation effects reduce the slope, even though a slower increase is still observed.[35] This decrease of the slope might indicate that non-radiative recombination or cascading processes are more important in this regime. This observation is unexpected since previously bimolecular or Auger recombination was reported for higher fluences.[36]

Further, from these fits, we determine the relative contribution of each phase to the overall PL signal for each fluence (Figure S5, Supporting Information). For all investigated fluences, ≈25–30% of the overall PL signal stem from the $n = 3$ RP-phase. This almost constant contribution from this phase strongly differs from the fluence-dependent contributions of the $n = 2$ and the $n \geq 4$ phases: While the contribution of the $n = 2$ increases exponentially with increasing fluence, the relative contribution of the $n \geq 4$ phase is reduced in a similar amount. This observation suggests a fluence-dependent cascading process from the low *n* RP phases to the high *n* phases as well as reduced availability of states in the low energy regime, which prevents fast relaxation processes.

For comparison, we recorded PL spectra with a higher excitation wavelength (reduced excess energy over the optical bandgap) of 515 nm (Figure 1c), to investigate the influence of photoexcitation energy on the luminescence. While experiments with excitation at 400 nm provide ≈1 eV excess energy over the optical bandgap of the $n = 2$ phase, this value is reduced to ≈200 meV for excitation at 515 nm.

We find that for 515 nm excitation mostly the $n \geq 4$ phases contribute to the PL signal. The PL spectra in Figure 1c further show different peak positions: the peak position for excitation under 515 nm is ≈10 nm redshifted compared to the spectra which were excited with 400 nm. This redshift is due to the emission

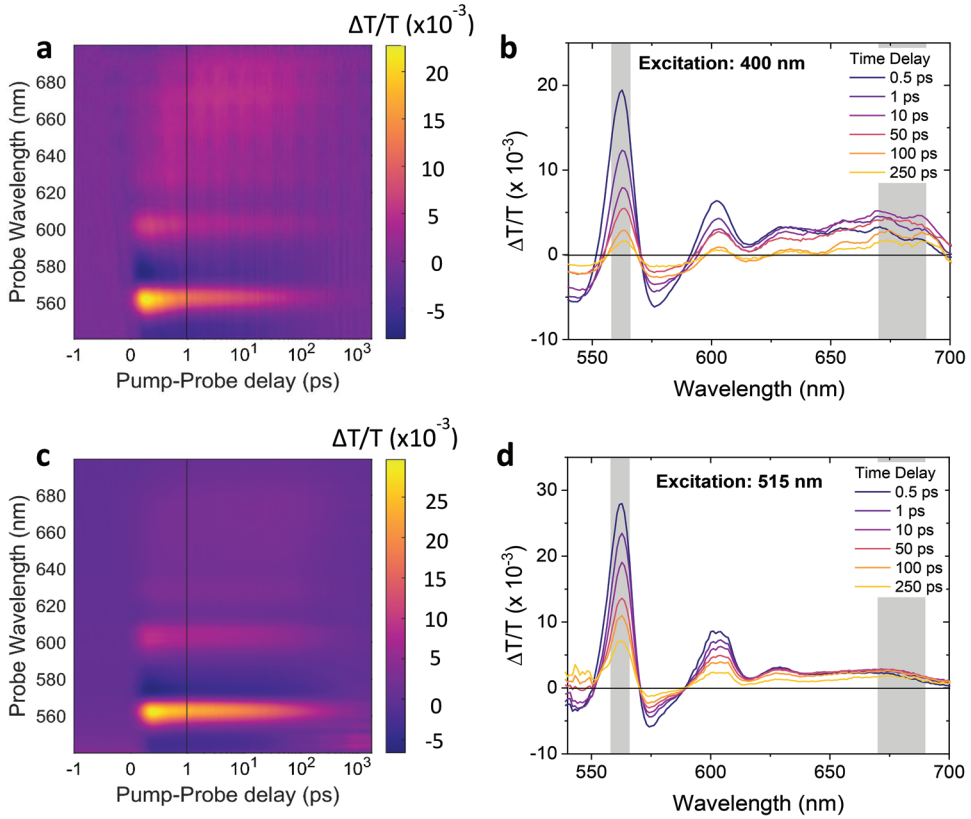

Figure 2. Transient absorption (TA) results for excitation wavelengths 400 and 515 nm, using a fluence of 3 μJ cm^{-2}: a,c): TA maps for (a) 400 nm and (c) 515 nm excitation showing a dominant ground state bleach GSB of the $n = 2$ phase at 560 to 565 nm, a GSB of the $n = 3$ phase near 605 nm and GSBs from the higher n phases at higher wavelengths at up to 700 nm. b,d): TA spectra for (b) 400 nm and (d) 515 nm excitation for selected time delays after excitations. Under excitation with 400 nm, stronger contributions to higher n-phases are found, indicating transfer of excitations to such phases on picosecond timescales. Unexpectedly, such transfer is reduced under 515 nm excitation, as evidenced by lower signal at higher wavelengths. The kinetics of the grey shaded areas are further analyzed in Figure 3.

originating from different phases: For 400 nm excitation, the peak at about 680 nm is a superposition of PL from multiple n-number phases, while for excitation at 515 nm the contribution from lower n-phases decreases drastically and the luminescence of phases with higher n-values becomes more pronounced.

Additionally, the peak intensity of the PL signal for a fluence of 30 μJ cm^{-2} is reduced by ≈74 % compared to the intensity for excitation at 400 nm at the same fluence. Since the PL intensity for excitation at 515 nm was very low, a higher fluence was chosen for this analysis. The spectra were corrected for differences in absorption for 400 and 515 nm excitation obtained from UV–vis measurements (Figure 1b; Figure S6, Supporting Information) as well as for the different numbers of photons corresponding to 30 μJ cm^{-2} for the different excitation wavelengths. This indicates that excitations in low-n phases now cascade faster than for excitation under 400 nm, and that these states are less luminescent after photoexcitation with low optical excess energy. This suggests an increase of non-radiative recombination processes for photoexcitation at 515 nm. We will further investigate the origin of this observation with transient absorption experiments as well as with time-resolved PL spectroscopy below.

To investigate the impact of the excess energy on luminescence in more detail, an excitation wavelength series of the PL spectra was recorded for the excitation wavelength range from 480 to 525 nm with fluences of ≈1.3 μJ cm^{-12}. A stark loss in signal intensity with increasing excitation wavelength was observed (Figure 1f). We note that the PL values were corrected for small variations of fluences and different absorption factors. For $n \geq 4$ phases, the PL signal intensity was reduced by ≈78 % while increasing the excitation wavelength from 480 to 525 nm, in agreement with the data shown in Figure 1c. Notably, for the $n = 3$ phase and the $n = 2$ phase, increasing the excitation wavelength from 480 to 525 nm caused a loss of signal intensity of > 80 %. For comparison, under excitation at 400 nm, photoluminescence quantum efficiency (PLQE) measurements showed a constant efficiency of ≈2 % (Figure S7, Supporting Information) for different irradiance intensities.

2.2. Results from Transient Absorption Spectroscopy

Next, we perform transient absorption (TA) measurements with 400 and 515 nm excitation (pump) (**Figure 2**a,c) to investigate the detailed origin of the effects we found in the PL spectra. For both excitation wavelengths, a fluence of ≈3 μJ cm^{-2} was chosen, which is in the excitation fluence regime that was investigated with PL (Figure 1d).

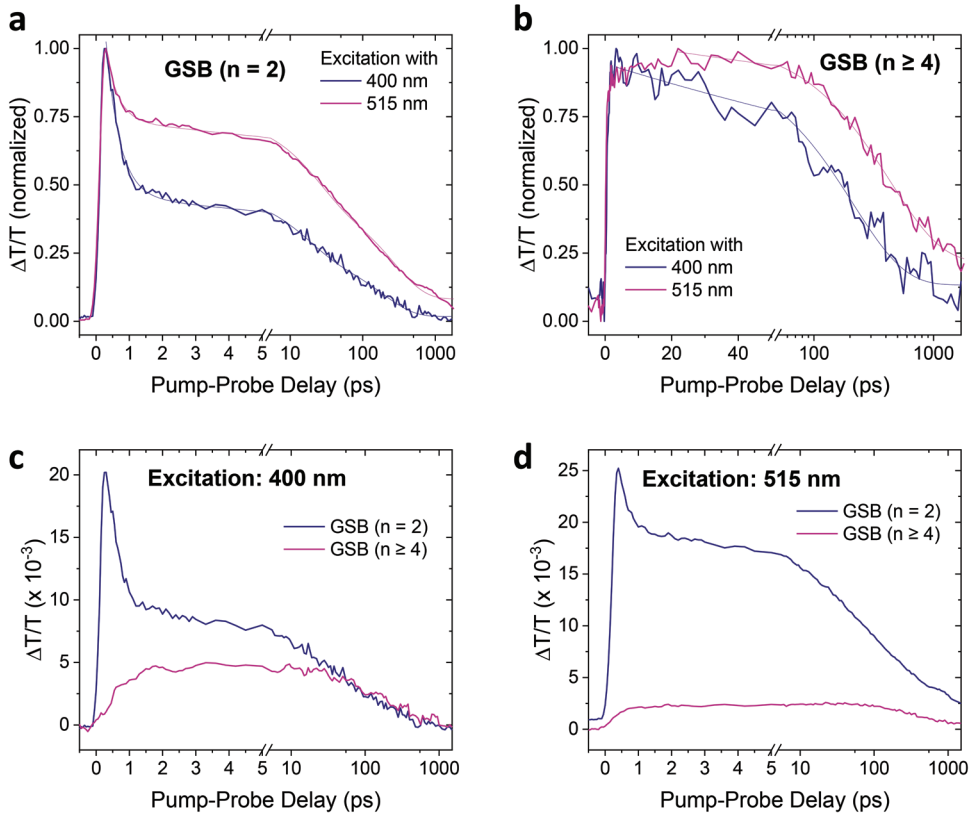

Figure 3. Recombination dynamics of a) high-energy optical bandgap ($n = 2$) and b) low-energy optical bandgap ($n \geq 4$) phases with suitable fits (thin lines). For 400 nm excitation, the GSB of the $n = 2$ phase decays faster than for 515 nm excitation . No concomitant rise in the low-bandgap phases is seen, indicating fast decay of excitations in the high-energy phases under 400 nm excitation. For excitation with 515 nm, a higher signal and longer rise times of signals in the low-energy phases are seen, indicating slower, but more pronounced, transfer of excitations. From the unnormalized kinetics c) and d) of the different GSB signals for excitation at 400 and at 515 nm one can recognize the reduced transfer from low *n*-RP phases to higher *n*-phases under excitation with 515 nm.

The TA spectra show a dominant ground state bleach (GSB) at 560 nm (corresponding to the RP phase $n = 2$) and additional bleaches for higher *n*-number RP phases at higher probe wavelengths. Notably, the strong GSB for $n = 2$, visible for both employed pump energies, suggests that the observed dependence of PL spectra on excitation wavelength cannot be simply explained by a difference in excitation population of the $n = 2$ phase.

Wavelength dependent TA spectra are shown for selected delay times in Figure 2b,d.

For excitation at 400 nm, we find a fast decrease of the GSB intensity of the $n = 2$ and $n = 3$ phase (Figure 2b). For the $n \geq 4$ phases, for which the GSB is located in the range of 625 to 700 nm, the signal intensity rises within the first tens of picoseconds. Additionally, the $n \geq 4$ signal shows an increasing redshift with time, which indicates a transfer to lower energy phases. In the $n \geq 4$ regime, the $n = 4$ phase can be clearly distinguished at ≈630 nm for both excitation wavelengths (Figure 2b,d). Higher *n*-number phases cannot be distinguished clearly any more due to the small energy differences between these phases.

For excitation with 515 nm (Figure 2d), we find a fast decrease of the GSB intensity for the $n = 2$ and $n = 3$ phases, similar to 400 nm excitation, but the $n \geq 4$ signal remains almost constant for all time delays. This indicates that not pronounced cascading into these phases occurs, and that photo-excitation densities do not change significantly with time delay. This suggests that the fast relaxation dynamics of the $n = 2,3$ phases under excitation at 515 nm must have a different origin than energy cascading. Combining the observed decrease of the GSB signal of the low n phases and the constant TA signal of the high n phases with the low PL for excitation under illumination at 515 nm, this hints at an increased relative amount of non-radiative recombinations.

While in the UV–Vis spectrum (Figure 1b) shows a small hint to the existence of the n = 1 phase in this material, no signal in this phase is found in the TA map for excitation with 400 nm (Figure S8, Supporting Information).

We next analyze the TA kinetics of the $n = 2$ phase to investigate the photoexcitation dynamics (**Figure 3**a). For both excitation wavelengths, the decay of the can be modeled with a three-exponential decay. The TA signal of the GSB decreases more strongly for excitation at 400 nm compared to excitation at 515 nm. For the 400 nm pump wavelength, the signal intensity decays by ≈50 % in the first picosecond followed by a faster biexponential decay, while for 515 nm pump wavelength, the signal drops only by ≈25 % in the first picosecond followed by a slower biexponential decay.

For both excitation wavelengths, the initial exponential decay has similar exponential decay time constant of ≈0.41 ps for 400 nm excitation and 0.35 ps for 515 nm excitation. This

decay is expected to be dominated from carrier relaxation and excitation-phonon interactions.[6,8] The similarity of these initial decay times suggests that phonon processes are more strongly influenced by the sample properties than by processes related to the different excitation wavelengths. On the other hand, the absolute decrease of signal intensity within the first picosecond depends on excess energy. This suggests that the phonon-scattering processes can only act on a sub-set of the photo-excitations under 515 nm excitation. For the following bi-exponential decay, the decay times are ≈16 ps and ≈186 ps for 400 nm excitation, and ≈22 and ≈267 ps for 515 nm excitation. This indicates that recombination or transfer of excitations with 400 nm photons is faster than for 515 nm excitation. Further, the persistent signal after 515 nm pump indicates that states remain excited in the $n = 2$ phase and that they can depopulate this phase only at a reduced rate compared to the 400 nm pumped sample.

Next, we analyze the TA kinetics of the higher number RP phases with $n \geq 4$ (Figure 3b). For 400 nm excitation, we find a fast rise of the signal within the first 10 to 20 ps, while for 515 nm excitation, the maximum intensity is reached only after ≈20 to 40 ps. These rise times agree with the decay times of 16 ps for excitation at 400 nm and 22 ps for excitation at 515 nm that were obtained for photoexcitations in the $n = 2$ phases, which likely relate to transfer processes of excitations from the $n = 2$ to the $n \geq 4$ phase. This cascading can be expected for multiphase layered hybrid perovskites based on previous reports.[33,34] For later times, both spectra show an exponential decay with a recombination time of 212 ps for 400 nm pump and 432 ps for 515 nm pump. Despite the decay times indicating transfer processes for both pump wavelengths, the absolute transfer efficiencies strongly differ for these materials (Figure 3c,d). For 400 nm excitation, the signal intensity of the $n = 2$ and the $n \geq 4$ phases show similar intensities for pump-probe delays larger than ≈50 ps, indicating transfer and population of the high *n*-number phases (Figure 3c). For 515 nm excitation, the $n = 2$ phase shows a stronger signal than the $n \geq 4$ phase for all investigated times. This hints at a reduced transfer from the $n = 2$ phase to higher *n*-number phases when pumping with 515 nm (or, conversely, a persistent population of the $n = 2$ phase), which appears to be in contrast to the weak signal from the $n = 2$ phase in PL spectra under 515 nm excitation.

Thus, we propose that photo-excitations formed under excitation with low optical excess energy are not contributing strongly to luminescence. Further, the stronger intensity loss in the $n = 2$ phase under excitation with 400 nm suggests that, unexpectedly, there is a recombination mechanism after 400 nm excitation, which outcompetes transfer to higher n-number phases and increases the PL signal from the low *n* phases. This indicates, that photo excitations in the $n = 2$ phase are more emissive if they are formed with excess energy. Furthermore, our findings show that the excess energy excitation is key for bright emission from higher *n*-number RP phases.

Charge transfer describes the transport of an electron (hole) into a higher n-number RP phase ("acceptor" phase), while a hole (electron) remains in the lower *n*-number RP phase ("donor" phase).

Comparing different GSBs in the TA spectrum is useful for probing charge transfer as the transfer of (free) charge carriers can be recognized from the rise of the newly populated phase without a simultaneous loss of the GSB of the phase the charge carrier is leaving from.[5]

We do not observe such a clear rise in the low-energy phases. Comparing the time-scales of our measured kinetics with literature and potential energy transfer mechanisms, our data hint at an ultrafast energy transfer via FRET. [25,33,37,38]

However, since our technique is not selectively probing free charges, we cannot completely rule out the occurrence of some contribution of charge transfer processes, especially on very short and very long time scales. Contributions from charge transfer processes could be further studied with methods particularly sensitive to the presence of free charges such as microwave conductivity measurements [39,40] or THz spectroscopy [41–43], as has been previously reported for hybrid perovskite materials.

2.3. Photoluminescence Kinetics

To gain insights into the underlying recombination mechanisms of the excitation dependent luminescence, we take time-resolved PL measurements. The temporal evolution of the PL intensity for the $n = 2$ phase (**Figure 4**a) and for the $n \geq 4$ phase (Figure 4b) strongly depends on the excitation wavelength. The rise time of the $n = 2$ phase for all investigated excitation wavelengths is below the temporal resolution of our set-up. Thus, we investigate the initial decay by determining the time it takes for the PL intensity to decay to $1/e \simeq 0.37$ of the initial peak intensity. This value is reached after 52 ps for 560 nm excitation, but only after 117 ps for excitation at 405 nm (inset in Figure 4a). This indicates that radiative rates can be controlled by excitation conditions in our material and that they remain higher for excess energy excitation conditions.

In comparison, in the TA kinetics of the $n = 2$ phase we found decay times of 16 ps for 400 nm excitation and 22 ps for 515 nm excitation, for the fast components of the biexponential decay, which describes transfer and recombination. While the TA decay times are decreasing for lower excitation wavelength, the recombination times in the PL decays are increasing. Additionally, we found from the TA kinetics for excitation at 515 nm (Figure 3a) that – despite some transfer to the higher *n*-phases – excited states remain in the $n = 2$ phase for long times. This indicates that – for excitation with excess energy - a larger fraction of the decay of the excitation population in the $n = 2$ phase is due to radiative recombination.

For the $n \geq 4$ phases (Figure 4b), the rise times strongly depend on the excitation wavelength. For resonant excitation at 560 nm, the maximum PL intensity only occurs after ≈1 ns, while for the other investigated wavelengths the signal peaks earlier. From exponential fits, we find rise times of ≈90 ps for excitation with 405 nm, ≈100 ps for excitation with 476/515 nm and 170 ps for excitation with 560 nm. The rise times of the PL of the $n \geq 4$ phase show an anti-correlation with the PL decay times of the $n = 2$ phase, and show the same trend as the decay times of the GSB from the n ≥ 4 phases in TA. This indicates a faster transfer into the $n \geq 4$ phases for excess energy excitation, e.g. faster cascading of the excitations with excess energy.

The decay times of the of the $n \geq 4$ phases decrease with higher excess energy excitation from 14.3 ns for resonant excitation at 560 nm to 3.5 ns for excitation with 405 nm (Figure S9,

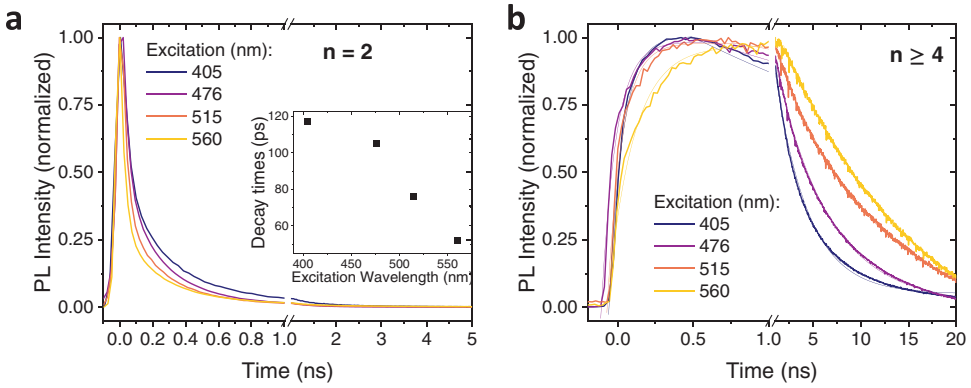

Figure 4. Impact of the excitation wavelength on the PL kinetics: For different n phases, normalized PL kinetics were obtained from time-dependent PL measurements a): For the $n = 2$ phase (detected at 570 nm), increasing the excitation wavelength leads to faster PL decay times with the corresponding decay times plotted in the inset. This decrease of the luminescence rate for higher excitation wavelengths indicates more non-radiative recombination. b): PL kinetics from the $n \geq 4$ phase (detected at 695 nm) show a slower rise and decay of the signal for longer excitation wavelengths, indicating higher luminescence rates. Thus, excitation with excess energy over the optical bandgap initiates stronger luminescent decay from high-n phases.

Supporting Information). This indicates that photoexcitations, which were formed with excess energy in the $n \geq 4$ phases states, recombine less strongly radiatively than upon excitation closer to the bandgap, where excited states are longer-lived in these low-bandgap phases and show a slower recombination rate, as evident from the slower decay time of the PL from the $n \geq 4$ phases.

We further investigate the spatial distribution of PL emission with confocal PL microscopy measurements (Figure S10, Supporting Information). We find that emission from the $n = 2$ phases is localized to smaller regions in the film, while emission from $n \geq 4$ phases is more homogeneously distributed throughout the sample. From these spatial distributions one would expect that emission from the high -*n*number phases outcompetes emission from lower -nphases at all times. Thus, our results indicate that the broadband emission which we found to arise from excess energy excitation requires a delicate interplay of recombination and transfer dynamics. Only if radiative decay from the $n = 2$ phase is sufficiently fast, it will outcompete transfer to the higher--- n-phases. On the other hand, we find that under these conditions, transfer dynamics into the higher n-number phases is increased. Overall, the enhancement in radiative rates outcompetes the increase in transfer rates, which yields the unusual broadband emission we have discovered.

3. Conclusion/Discussion

We have shown, that the PL spectra of our multiphase sample strongly depend on the excitation wavelength. For excitation with 405 nm pump, a much stronger signal from low n-RP phases and especially from the $n = 2$ phase, has been observed than under excitation with 515 nm or resonant excitation. Combing the comparable fast decay of the TA GSB signal for the $n = 2$ phase and the long lifetimes of PL upon excitation with 400 nm, this hints at excitations going through a radiative, fast channel rather than transferring to optically less active states for excitation at 400 nm. On the other hand, for excitation at 515 nm, the short-lived PL signal from $n = 2$ and the long lasting GSB signal for the $n = 2$ phase indicate more non-radiative recombination.

The long lifetimes of PL signal from different RP phases upon excitation with 405 nm are too long to be explained with the investigated TA GSB signal. The long lifetimes of the $n \geq 4$ phases upon excitation with 515 nm also exceed the analyzed timescales of the TA signal. The observations for PL for timescales later than 1.5 ns might therefore be related to different processes.

Comparing the decay times for TA and PL indicate that a significant share of the loss of the $n = 2$ GSB signal could be due radiative recombination of this phase. Analyzing the PL kinetics of different n -phases, transfer to higher n-phases could be found. Our observations could be explained by the formation of optically less active excitons after excitation with 515 nm, which cannot decay as long as they are exciton-like states in the low n-phases, but become brighter for recombination from higher n-phases, where they are more free-carrier-like. For excitation at 400 nm, all radiative decay and transfer processes happen faster. The combined effect is that for a 400 nm photoexcitation the samples emit from all phases more equally.

Furthermore, the PL from low n phases is not only for excitation at 515 nm very low, but also for excitation at 400 nm with very low fluences, which hints at phonons, e.g. generated during the thermalization of hot excitons after excitation with excess energy, being important for the brightening of the low n phases.

A possible mechanism for explaining our observations is an excitation energy dependent population of strongly emissive states (e.g., states with strong electron-hole-overlap or spin-allowed recombination) and weakly emissive states (e.g., with low electron-hole-overlap or spin-forbidden recombination). Such weakly emissive states can be triplet excitons, exciton-polarons or weakly bound excitons. We find that increasing excess energy enhances the population of the strongly emissive states in our materials. Optical excess energy typically results in the formation of hot excitations which cool down to the lowest energy electronic states in their respective RP phases through cooling (phonon emission) and thermalization (phonon/carrier scattering) processes. The observation that excess energy is required to obtain strong radiative emission suggests that activation energy is required to populate the strongly emissive states from energetically lower weakly emissive states. We take this as a sign that

weakly emissive states with lower energy exist in the material that can be excited into the brightly emissive states through phonon interactions.

A key difference hereby is that due to the larger amount of excess energy provided by the excitation with 400 nm, more phonons are created during the cooling process than after an excitation at 515 nm. These play a key role in overcoming the energy barrier between strongly and weakly emissive states in the lower n-phases. Hence, for excitation with 400 nm more excited states can be transferred into the strongly emissive state, explaining the observed brightening of the $n = 2$ and $n = 3$ phase after photoexcitation at 400 nm.

In contrast, upon excitation with 515 nm, the excess energy of photons over the bandgap is lower, thus, there will be a reduced activation of phonon modes which is then not sufficient to significantly populate the $n = 2$ strongly emissive states anymore.

Within one RP phase relaxed states either decay through radiative/non-radiative processes or transfer to neighboring phase-domains. Here, we need to consider that these transfers of photo-excitations occur from lower n-number RP phases into higher n-number RP phases with lower bandgap. Due to the resulting Type I band alignment, the transferred excitations gain excess energy over the band gap in the "acceptor" RP phase. As observed for excitation with 400 nm in the $n = 2$ phase, we expect that this results in a cooling process which enables more states to populate the strongly emissive, which then leads to the observed bright emission from the higher n-number RP phases.

Brightening of high bandgap phases in multiphase perovskites via excitation with excess energy is a simple way to control the individual contributions to the overall PL spectrum and could hence be a promising potential approach for light-emitting applications.

4. Experimental Section

The experimental section can be found in the supporting information.

Supporting Information

Supporting Information is available from the Wiley Online Library or from the author.

Acknowledgements

This project has received funding from the Deutsche Forschungsgemeinschaft (DFG) under Emmy Noether Program (Project 387651688). F.D. and A.S. acknowledge financial support from the Deutsche Forschungsgemeinschaft (DFG) under the Emmy Noether Program (Project 387651688). S.F. was grateful for support from the Rowland Institute at Harvard. A.H. acknowledges financial support from the from the Deutsche Forschungsgemeinschaft (DFG) through Germany's Excellence Strategy-EXC 2089/1-390776260. M.-W.H., S.L., and J.Z. acknowledge funding from the European Research Council (ERC Starting Grant agreement no. 852084 — TWIST). Figure 4a has been replaced by the proper version on March 13, 2024 after original online publication.

Open access funding enabled and organized by Projekt DEAL.

Conflict of Interest

The authors declare no conflict of interest.

Data Availability Statement

The data that support the findings of this study are available from the corresponding author upon reasonable request.

Keywords

broad photoluminescence spectrum, $n = 2$ perovskites, multi-phase emission, optically passive states, photoexcess energy, quasi 2D lead iodide perovskites

Received: June 6, 2023
Revised: September 8, 2023
Published online: October 2, 2023

[1] Y. Li, X. Luo, Y. Liu, X. Lu, K. Wu, *ACS Energy Lett.* **2020**, *5*, 1701.
[2] C. C. Stoumpos, D. H. Cao, D. J. Clark, J. Young, J. M. Rondinelli, J. I. Jang, J. T. Hupp, M. G. Kanatzidis, *Chem. Mater.* **2016**, *28*, 2852.
[3] X. Li, J. M. Hoffman, M. G. Kanatzidis, *Chem. Rev.* **2021**, *121*, 2230.
[4] S. A. Bourelle, F. V. A. Camargo, S. Ghosh, T. Neumann, T. W. J. Van De Goor, R. Shivanna, T. Winkler, G. Cerullo, F. Deschler, *Nat. Commun.* **2022**, *13*, 3320.
[5] J. M. Richter, F. Branchi, F. Valduga De Almeida Camargo, B. Zhao, R. H. Friend, G. Cerullo, F. Deschler, *Nat. Commun.* **2017**, *8*, 376.
[6] M. Li, J. Fu, Q. Xu, T. C. Sum, *Adv. Mater.* **2019**, *31*, 1802486.
[7] Y.i Zhang, X. Jia, S. Liu, B.o Zhang, K. Lin, J. Zhang, G. Conibeer, *Sol. Energy Mater. Sol. Cells* **2021**, *225*, 111073.
[8] J. W. M. Lim, Y. Wang, J. Fu, Q. Zhang, T. C. Sum, *ACS Energy Lett.* **2022**, *7*, 749.
[9] M. Nuber, D. Sandner, T. Neumann, R. Kienberger, F. Deschler, H. Iglev, *J. Phys. Chem. Lett.* **2021**, *12*, 10450.
[10] M. Gramlich, M. W. Swift, C. Lampe, J. L. Lyons, M. Döblinger, A. L. Efros, P. C. Sercel, A. S. Urban, *Adv. Sci.* **2022**, *9*, 2103013.
[11] M. Dyksik, H. Duim, D. K. Maude, M. Baranowski, M. A. Loi, P. Plochocka, *Sci. Adv.* **2021**, *7*, 46.
[12] N. Mondal, A. De, S. Seth, T. Ahmed, S. Das, S. Paul, R. K. Gautam, A. Samanta, *ACS Energy Lett.* **2021**, *6*, 588.
[13] K. Xu, J. F. Vliem, A. Meijerink, *J. Phys. Chem. C* **2019**, *123*, 979.
[14] M. A. Becker, R. Vaxenburg, G. Nedelcu, P. C. Sercel, A. Shabaev, M. J. Mehl, J. G. Michopoulos, S. G. Lambrakos, N. Bernstein, J. L. Lyons, T. Stöferle, R. F. Mahrt, M. V. Kovalenko, D. J. Norris, G. Rainò, A. L. Efros, *Nature* **2018**, *553*, 189.
[15] M. Koperski, M. R. Molas, A. Arora, K. Nogajewski, M. Bartos, J. Wyzula, D. Vaclavkova, P. Kossacki, M. Potemski, *2D Mater.* **2019**, *6*, 015001.
[16] A. Y. Joe, L. A. Jauregui, K. Pistunova, A. M. Mier Valdivia, Z. Lu, D. S. Wild, G. Scuri, K. De Greve, R. J. Gelly, Y. Zhou, J. Sung, A. Sushko, T. Taniguchi, K. Watanabe, D. Smirnov, M. D. Lukin, H. Park, P. Kim, *Phys. Rev. B* **2021**, *103*, L161411.
[17] M. M. Elshanawany, A. G. Ricciardulli, M. Saliba, J. Wachtveitl, M. Braun, *Nanoscale* **2021**, *13*, 15668.
[18] Y. Yu, C. Zhao, L. Ma, L. Yan, B.o Jiao, J. Li, J. Xi, J. Si, Y. Li, Y. Xu, H. Dong, J. Dai, F. Yuan, P. Zhu, A. K.-Y. Jen, Z. Wu, *J. Phys. Chem. Lett.* **2022**, *13*, 3674.
[19] B. Segall, G. D. Mahan, *Phys. Rev.* **1968**, *171*, 935.
[20] R. M. Kolbas, N. Holonyak, B. A. Vojak, K. Hess, M. Altareli, R. D. Dupuis, P. D. Dapkus, *Solid State Commun.* **1979**, *31*, 1033.
[21] L. Dusanowski, A. Musial, G. Sek, P. Machnikowski, *Acta Phys. Pol. A* **2013**, *124*, 813.
[22] S. Brem, A. Ekman, D. Christiansen, F. Katsch, M. Selig, C. Robert, X. Marie, B. Urbaszek, A. Knorr, E. Malic, *Nano Lett.* **2020**, *20*, 2849.

[23] M. Yuan, L.i N.a Quan, R. Comin, G. Walters, R. Sabatini, O. Voznyy, S. Hoogland, Y. Zhao, E. M. Beauregard, P. Kanjanaboos, Z. Lu, D. H.a Kim, E. H. Sargent, *Nat. Nanotechnol.* **2016**, *11*, 872.
[24] K. Zheng, Y. Chen, Y. Sun, J. Chen, P. Chábera, R. Schaller, M. J. Al-Marri, S. E. Canton, Z. Liang, T. Pullerits, *J. Mater. Chem. A* **2018**, *6*, 6244.
[25] A. H. Proppe, M. H. Elkins, O. Voznyy, R. D. Pensack, F. Zapata, L. V. Besteiro, L.i N.a Quan, R. Quintero-Bermudez, P. Todorovic, S. O. Kelley, A. O. Govorov, S. K. Gray, I. Infante, E. H. Sargent, G. D. Scholes, *J. Phys. Chem. Lett.* **2019**, *10*, 419.
[26] Y. Jiang, J. Wei, M. Yuan, *J. Phys. Chem. Lett.* **2021**, *12*, 2593.
[27] J. Zhang, X. Zhu, M. Wang, B. Hu, *Nat. Commun.* **2020**, *11*, 2618.
[28] M. Bidikoudi, E. Fresta, R. D. Costa, *Chem. Commun.* **2018**, *54*, 8150.
[29] G. Yang, X. Liu, Y. Sun, C. Teng, Y. Wang, S. Zhang, H. Zhou, *Nanoscale* **2020**, *12*, 1571.
[30] J. Chen, J. Wang, X. Xu, J. Li, J. Song, S.i Lan, S. Liu, B.o Cai, B. Han, J. T. Precht, D. Ginger, H. Zeng, *Nat. Photonics* **2021**, *15*, 238.
[31] J. Leng, T. Wang, Z.-K. Tan, Y.a-J.u Lee, C.-C. Chang, K. Tamada, *ACS Omega* **2022**, *7*, 565.
[32] Z. Ren, K. Wang, X. W. Sun, W. C. H. Choy, *Adv. Funct. Mater.* **2021**, *31*, 2100516.
[33] M. E. F. Bouduban, A. Burgos-Caminal, R. Ossola, J. Teuscher, J.-E. Moser, *Chem. Sci.* **2017**, *8*, 4371.
[34] F. Zhang, B. Cai, J. Song, B. Han, B. Zhang, H. Zeng, *Adv. Funct. Mater.* **2020**, *30*, 2001732.
[35] N. Mondal, R. Naphade, X. Zhou, Y. Zheng, K. Lee, I. Gereige, A. Al-Saggaf, O. M. Bakr, O. F. Mohammed, Y. N. Gartstein, A. V. Malko, *J. Phys. Chem. Lett.* **2020**, *11*, 1112.
[36] K. P. Goetz, A. D. Taylor, F. Paulus, Y. Vaynzof, *Adv. Funct. Mater.* **2020**, *30*, 191004.
[37] Q.i Zhang, E. Linardy, X. Wang, G. Eda, *ACS Nano* **2020**, *14*, 11482.
[38] S. Panuganti, L. V. Besteiro, E. S. Vasileiadou, J. M. Hoffman, A. O. Govorov, S. K. Gray, M. G. Kanatzidis, R. D. Schaller, *J. Am. Chem. Soc.* **2021**, *143*, 4244.
[39] Y. Bi, E. M. Hutter, Y. Fang, Q. Dong, J. Huang, T. J. Savenije, *J. Phys. Chem. Lett.* **2016**, *7*, 923.
[40] D. Bartesaghi, A. H. Slavney, M. C. Gélvez-Rueda, B. A. Connor, F. C. Grozema, H. I. Karunadasa, T. J. Savenije, *J. Phys. Chem. C* **2018**, *122*, 4809.
[41] R. L. Milot, R. J. Sutton, G. E. Eperon, A. A. Haghighirad, J. Martinez Hardigree, L. Miranda, H. J. Snaith, M. B. Johnston, L. M. Herz, *Nano Lett.* **2016**, *16*, 7001.
[42] L. M. Herz, *ACS Energy Lett.* **2017**, *2*, 1539.
[43] S. G. Motti, J. B. Patel, R. D. J. Oliver, H. J. Snaith, M. B. Johnston, L. M. Herz, *Nat. Commun.* **2021**, *12*, 6955.